energies

Article

Analysis of an Evaporative Condensation System Coupled to a Microchannel-Separated Heat Pipe for Data Centers

Ying Wang [1], Xiang Huang [1,*], Junjie Chu [1], Yan Du [1], Xing Tang [2], Cong Dai [1] and Gang Ma [1]

[1] School of Urban Planning and Municipal Engineering, Xi'an Polytechnic University, Xi'an 710048, China
[2] BLUE-ON (Jiangsu) Environmental SYSTEM Co., Ltd., Taixing 225441, China
* Correspondence: huangx@xpu.edu.cn

Abstract: In the age of the digital economy, the data center is the most crucial piece of infrastructure. The issue of the excessive power consumption of a data center's cooling system needs to be addressed as the national objective of "peak carbon and carbon neutrality" is increasingly promoted. In this study, a microchannel-separated heat pipe-cooling system with evaporative condensation is introduced. The system may switch between three modes of operation in response to changes in outdoor air quality parameters, thereby maximizing the utilization of natural cooling sources while lowering data centers' cooling costs. The purpose of this paper is to analyze the energy-saving potential of the hybrid system through experimental tests. The results show that 114.4% is the ideal liquid-loading rate for the heat pipe system. Under working conditions in Xi'an, the annual operating hours of the three modes accounted for 47.2%, 6.1%, and 46.7%. The hybrid cooling system may save 62.04% of the energy used annually compared to the standard cooling system and the cooling system in the server room thanks to its yearly average COP of 9.43.

Keywords: data center; microchannel separate heat pipe; evaporative condensation; performance test

Citation: Wang, Y.; Huang, X.; Chu, J.; Du, Y.; Tang, X.; Dai, C.; Ma, G. Analysis of an Evaporative Condensation System Coupled to a Microchannel-Separated Heat Pipe for Data Centers. *Energies* **2022**, *15*, 9056. https://doi.org/10.3390/en15239056

Academic Editor: Álvaro Gutiérrez

Received: 23 October 2022
Accepted: 20 November 2022
Published: 30 November 2022

1. Introduction

In the context of the rapid development of the global digital economy and the change in the endemic New Crown Pneumonia epidemic, countries have begun to perceive the digital economy as a key means of achieving economic recovery and promoting transformation and upgradation. The pace of economic development has accelerated from physical space to digital space, gradually moving from land, labor, and machines to data, algorithms, and arithmetic power. A data center is the arithmetical infrastructure for storing, processing, and using data, typically consisting of power supply and cooling, IT technology, load and application software, energy efficiency management, and so on. As of 2019, the Chinese government, companies, educational institutions, etc., have approximately 74,000 rooms of various types of data centers, representing 23% of the total number of data centers in the world. Relevant data from the Ministry of Industry and Information Technology of China shows that in 2021 the total size of the racks of data centers in use in China was 5.2 million racks of standard data, the average shelving rate of 55% yielded a total IT load of 7150 MW, and the total power consumption of the data centers was 94 billion KWh. The total electricity consumption of data centers in China is projected to be in excess of 180 billion KWh by 2030, or 1.5~2.0% [1,2].

In addition to the quantity and size, cooling energy use accounts for between 30% and 50% of the share of energy use in data centers [3–5]. Traditional data center-cooling equipment includes a computer room air conditioning unit (CRAC) based on mechanical vapor compression refrigeration, which suffers from high power consumption, low utilization, high PUE (power usage effectiveness), and a large footprint. CRACs need to run 24 h a day in order to meet the cooling requirements of data rooms. Even if a natural cooling source is not fully utilized, a CRAC's energy consumption and O&M expenses are not even appropriately comparable to the expense of purchasing new servers [6]. In the face of PUE's crucial import in recent years, and based on the premise of ensuring the environmental requirements of the server room and the safety and reliability of the cooling system, the full utilization of natural cooling sources and the expansion of the application areas and utilization time of these sources can realize greater benefits by promoting energy savings and emissions reductions in data centers.

Some of the main forms of natural data center-cooling systems' applications include direct/indirect air-side cooling, water-side cooling, and natural heat pipe cooling [7,8]. Natural cooling technology on the air side constitutes the introduction of cold, outside air into the data center either directly or via enthalpy cooling such as using a wet film (also known as direct evaporative-cooling technology). This approach reduces the energy consumption of the data center's cooling system through the direct exchange of heat and moisture between indoor and outdoor heat and cooling sources, which has the features of a simple structure, low cost, and high power efficiency. The energy-saving effect of this technology has been confirmed in the Facebook data center in Prineville, Oregon, USA; the Shirakawa data center in Fukushima, Japan; and the Amazon cloud-computing data center in Zhong Wei Western Cloud Base, Ningxia, China [9–12]. High outdoor air quality is required for this solution, and if moisture, dust, and acidic gases are trapped in the air, this can lead to fluctuations in indoor environmental parameters and even cause damage to the IT equipment in the data center.

On the water side, natural cooling technology can cool a data center directly with cold ambient water or indirectly with low-temperature water obtained by using cooling towers and dry coolers. The Dong Jiang Lake data center uses fresh river water for cooling, and its servers can be cooled by natural river water-based-cooling technology for over 90% of the year with a mean annual PUE of 1.15 [13]. Alibaba's data center in Qian Dao Lake uses lake water as a source of free cooling with a mean annual PUE of less than 1.3 [14]. Google's data center in Hamina, Finland, uses cold, deep-sea water from the Baltic Sea for cooling purposes with a mean annual PUE of approximately 1.14 [15]. The direct use of cold environmental water as a cooling source enables significant energy savings. However, the spread of this technology in data centers is still not widespread because of resource conditions, ecological protection, and geographical constraints.

Natural, indirect cooling technology on the air side uses external cooling sources through heat exchangers. This avoids direct air contact between the indoor and outdoor environments and can effectively ensure air humidity and cleanliness requirements in the data room. Indirect evaporative cooling (IEC) is a technology widely preferred by data centers because it reduces the temperature of the outlet air without changing the moisture content of the air by means of inter-wall heat transfer. The Tencent T block data center [16] used a natural air-side indirect cooling system based on an indirect evaporative-cooling heat exchanger to significantly reduce the power consumption of the cooling system, achieving a mean annual PUE of approximately 1.10. The National Snow and Ice Data Center (NSIDC) [17,18] used a system of indirect evaporative cooling to fully retrofit the CRAC system. Along with the cooling capacity needed to meet the constant data center load, the energy consumption from operating the cooling system was reduced by over 70% in summer and over 90% in winter. Ham [12] investigated the potential for energy savings from various natural air-side coolers for data center applications. The results showed savings of 76% to 99% in the cooling coil load and 47.5% to 67.2% in the total cooling energy of the system when compared to a conventional cooling system (CRAC) in a data center. The energy savings of indirect air-side natural cooling with high-efficiency heat exchangers were significant (63.6%). Yin Bi [19] et al. conducted an example analysis of the energy consumption and energy use efficiency of new indirect evaporative cooling systems for data centers of different sizes under different climatic conditions based on the cooling load of data centers. The electricity consumption savings from the data centers' air conditioning systems in the selected 10 climates ranged from 87.7% to 91.6% in 10 typical cities. Robert Tozer [20] explored the potential to achieve zero-energy cooling for data center applications in the United States. The results show that for many western U.S. cities, zero-energy cooling can be achieved using indirect air-side natural cooling within the ASHRAE A1 allowable supply air temperature range. Evaporative cooling is a technology in which water is used as a coolant to reduce the temperature of the cooled medium directly or indirectly through the natural property of the evaporation and absorption of heat when water is in direct contact with air. This method can produce significant energy-saving benefits in dry climates. Unfortunately, however, water resources are relatively scarce in areas where dry-air energy is abundant, and the units have high water use demands [21] and require high water quality. In addition, as operating life is extended, water quality issues will lead to the scaling of the heat exchange core area or cause a decrease in the heat exchange efficiency of the device. In addition, the units are large, and the limitation of their installation number will affect the installed capacity of data center cabinets, regardless of whether indoor, outdoor, or rooftop installation forms are used.

A heat pipe relies on the phase change of the working fluid within the pipe to achieve heat transfer and can be divided into two types: an integral heat pipe and a separated heat pipe. Due to the flexibility of installed split heat pipes, they are more mature than monolithic heat pipes. When fitted with a mechanical pump to increase the driving force for the flow, power-split heat pipe systems can operate in data centers with long duct lengths, large height differences, multiple branches, large heat fluxes, or limitations in installation [22,23]. In addition, compared to natural direct cooling on the air side, this system does not require the direct introduction of outside air, thereby avoiding the former problem of equipment failure due to contamination by outdoor particulate matter and uncontrolled humidity. Compared to natural cooling on the water side, it achieves efficient phase change heat transfer, overcoming limitations in water sources and application scenarios. Compared to natural indirect cooling on the air side, this system has a simple structure and is not limited by the former's high water quality, installation, application, and maintenance costs [24].

While powered split heat pipe systems can make effective use of natural cooling sources, when the outdoor air temperature is high, they must still rely on a mechanical cooling system for support [25,26]. Therefore, there is a need to search for new cooling methods to extend heat pipe systems' duration of cooling and reduce the cooling energy consumption of data centers.

Heat pipe technology and evaporative cooling are both energy-saving and environmentally friendly cooling technologies. However, given that heat pipe technology can only be used when outdoor air temperatures are low, evaporative cooling technology can effectively reduce outdoor air temperatures when outdoor temperatures are high. For this reason, this paper proposes a refrigeration system employing evaporative condensing and the microchannel-separated coupling of heat pipes for data centers. This is achieved by using a microchannel heat exchanger to increase the heat transfer performance of the heat pipe combined with the efficient cooling technology of evaporative condensation. Not only can it extend the use time of the natural cooling source, but it also saves system space by integrating both to achieve hardware integration and system simplification. This system can meet data centers' air supply requirements and produces large energy-saving effects.

2. Description of Complex Evaporative-Condensing and Microchannel-Separated Heat Pipe Unit

2.1. Evaporative-Condensing and Microchannel-Separated Heat Pipe Unit

The main components of the unit are the separated micro-channel heat pipe unit, evaporative-condensing unit, mechanical refrigeration make-up cooling unit, two primary supply fans, four secondary exhaust fans, one set of spray water delivery devices, one circulating water pump, one water storage tank, one water flow meter, and associated water pipes, valves, filters, and so on. The physical schematic of the unit is shown in Figure 1.

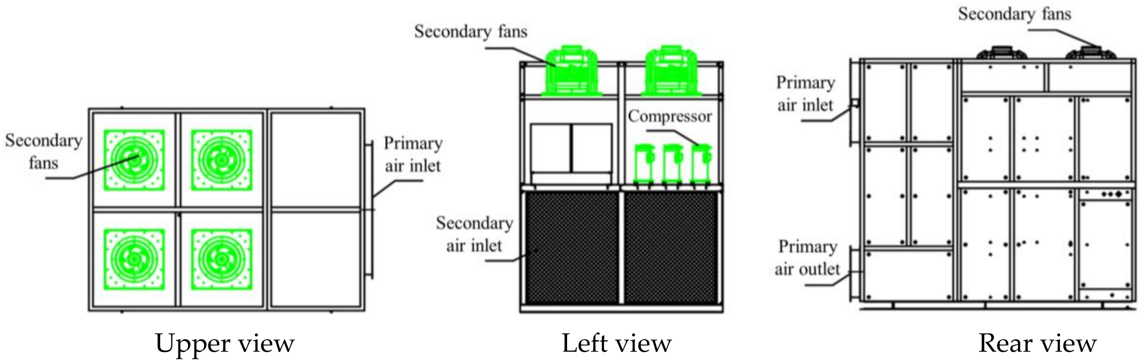

Figure 1. Physical schematic of the unit.

The separated heat pipe microchannel system consists of a heat pipe evaporator, a heat pipe condenser, a reservoir, and a fluorine pump, and is composed of two parts. With the aim of reducing the thermal resistance of the heat pipe [27] and the footprint of the device, the evaporator and condenser are arranged in a tilted position with a tilt angle of 45°. The fin spacing of the microchannel heat pipe condenser used in the evaporative condenser unit is close (1.3 mm), and the spray water is in direct contact with the fins according to the traditional method of direct spraying. If the water quality of the spray is poor, it will easily lead to scaling on the surface of the fins and increase the heat transfer resistance of the fins. For this reason, the method of pre-cooling the wet film has been adopted, the filler is arranged at an angle of 45° (filler size: 2400 mm × 2160 mm × 150 mm), and the sputtering water is sprayed onto the wet film. The outside air is cooled by the wet film and then passes through the condenser of the heat pipe, carrying only a trace of the water droplets in the air. Not only can this avoid the scaling of the fin area during long-time operation but it can also appropriately reduce the fin spacing and increase the number of fins in the condenser in order to increase the effect of heat exchange.

For this experiment, seven air condition measurement points were established. The measurement points on the secondary air side primarily consists of a secondary air inlet, after wet-film pre-cooling, after heat pipe condenser, and a secondary air outlet. The primary air side consists primarily of a primary air inlet, a heat pipe evaporator, and a primary air outlet. The operating parameters of the collected air include the dry-bulb temperature, relative humidity, flow rate, and pressure drop. Table 1 shows the specifications of the different measurement instruments.

Table 1. Specifications of various measuring instruments.

Parameter	Device	Range	Accuracy	Quantity
Dry-bulb temperature	RHLOG-T-H	−25~55 °C	±0.3 °C	8
Relative humidity	E + E210	2~98% RH	±2.5%	8
Air velocity	SwemaAir300	0.1~30 m/s	±0.1 m/s	5
Air pressure meter	Setra266	0~250 Pa	±1% FS	2
Water meter	LYH-8	0~600 L/h	±0.005 L	1
Fan power meter	ABB, M2 M LCD	0~60 kW	±1%	6
Pump power meter	TTi, EL155RDC	0~2 kW	±0.5%	2

2.2. Design Parameters of the Hybrid Cooling System

These parameters are based on the data center design specification (GB50174-2017) [28] stipulating the requirements for the hot and humid environment of a data center's server room, for example, the temperature of the entrance area of the cold aisle or cabinet is 18~27 °C, the dew point temperature is 5.5~15 °C, and the relative humidity does not exceed 60%. When IT equipment can operate under relaxed ambient temperature and relative humidity requirements, in order to conserve energy, the temperature of the cold aisle or the air entry area of the server room can be raised to 15~32 °C.

The unit has a nominal cooling capacity of 120 kW, an air supply temperature of 25 °C, a relative humidity of 50%, and a refrigerant load in the heat pipe of R22. If the outdoor dry-bulb temperature is below 14 °C, the heat pipe can support the entire cooling load, and the condensing temperature is set to 22 °C; the fluorine pump will cause the evaporating temperature of the heat pipe to be slightly higher than the condensing temperature, so take the evaporating temperature will be 22.5 °C. Table 2 shows the design parameters for the unit.

Table 2. Unit design parameters.

Parameters	Unit	Value
Cooling capacity Q	kW	120
Heat pipe condenser inlet air temperature $t_{0,m}$	°C	14
Heat pipe evaporator inlet air temperature t_1	°C	38
Primary air volume (machine room return air) M_1	m^3/h	30,000
Secondary air volume (outdoor fresh air) M_2	m^3/h	66,000
Primary return air temperature/humidity t_1/φ_1	°C/%	38 °C/25%
Primary air supply temperature/humidity t_2/φ_2	°C/%	25 °C/50%
Condensation temperature of the working mass t_c	°C	22
Workpiece evaporation temperature t_e	°C	22.5
Mass flow rate of the working mass G	kg/s	0.606

2.3. Hybrid Cooling System Operation Mode

Depending on the aperture of each functional section, the evaporative condensing and microchannel-separated heat pipe unit has three modes of operation. The switching points for each mode of operation are given in Table 3.

(1) Power heat pipe mode

When the outdoor dry-bulb temperature is lower than 14 °C, the first and second ventilators and fluorine pumps are switched on, and both the evaporative condenser unit and the mechanical refrigeration unit cease to function. The return air from the machine room is treated by the heat pipe evaporator to maintain the relative humidity, is cooled down, and then sent back to the machine room. At this time, the new outdoor air is treated by the heat pipe condenser to maintain the relative humidity and is then discharged from the unit after it is warmed up.

(2) Evaporative condensing and power heat pipe mode

When the outdoor dry-bulb temperature is higher than 14 °C and the wet-bulb temperature is less than 13 °C, the evaporative condenser unit is switched on based on the power heat pipe mode. The outdoor fresh air is first cooled down under the condition of maintaining the same enthalpy through the wet film and then reaches the heat pipe condenser to maintain the same relative humidity while warming up and discharging the unit. The return air treatment process of the machine room is the same as the power heat pipe mode.

(3) Mechanical refrigeration make-up cooling unit

When the outdoor dry-bulb temperature is higher than 14 °C and the wet-bulb temperature is higher than 13 °C, the mechanical refrigeration section switches on the appropriate number of compressors (a total of four units, accounting for 10~50% of the supplementary cooling capacity) according to the return air temperature of the machine room at this time. The fresh outdoor air is first cooled down by the wet film under the premise of maintaining the same enthalpy and then reaches the heat pipe condenser and mechanical refrigeration condenser and is discharged from the unit after two constant relative humidity and temperature increases. The return air from the machine room is first pre-cooled by the heat pipe evaporator and then sent back to the machine room after the second cooling procedure by the mechanical refrigeration evaporator.

Table 3. Unit operation mode.

Operation Mode	Fluorine Pumps	Compressors	Circulating-Water Pump	Outdoor Air Conditions
Power Heat Pipe	Open	Close	Close	$t_d \leq 14$ °C
Power heat pipe and evaporative condensing	Open	Close	Open	$t_d > 14$ °C and $t_w \leq 13$ °C
Mechanical refrigeration-based cooling	Open	Open	Open	$t_d > 14$ °C and $t_w > 13$ °C

3. Design of Separated-Microchannel Heat Pipe

3.1. The Dimensions of the Microchannel Heat Exchangers

The microchannel heat exchanger can effectively improve the heat transfer coefficient compared with the traditional heat exchanger, so both the evaporator and condenser of the heat pipe use the microchannel heat exchanger. The overall structure of the heat exchanger is shown in Figure 2, which is primarily composed of flat tubes, collector tubes, and louvered fins. The dimensions of the single flat tube are shown in Figure 3, and the specific structural parameters are shown in Table 4.

Table 4. Microchannel heat exchanger's structural size parameters.

Structure Parameters	Value (mm)	Structure Parameters	Value (mm)
Flat tube outer width B_{to}	36	Fin width B_f	36
Flat tube inner width B_{ti}	34.6	Fin height H_f	8
Flat tube outer height H_{to}	2	Fin pitch P_f	1.3
Flat tube inner height H_{ti}	1.34	Shutter angle the t_a	30°
Number of flakes N_w	25	Shutter length L_1	6.8
Sheet thickness δ_w	0.37	Shutter spacing P_1	1
Flat pipe spacing A	10	Fin thickness δ_f	0.08
Thickness of flat tube δ_r	0.33		

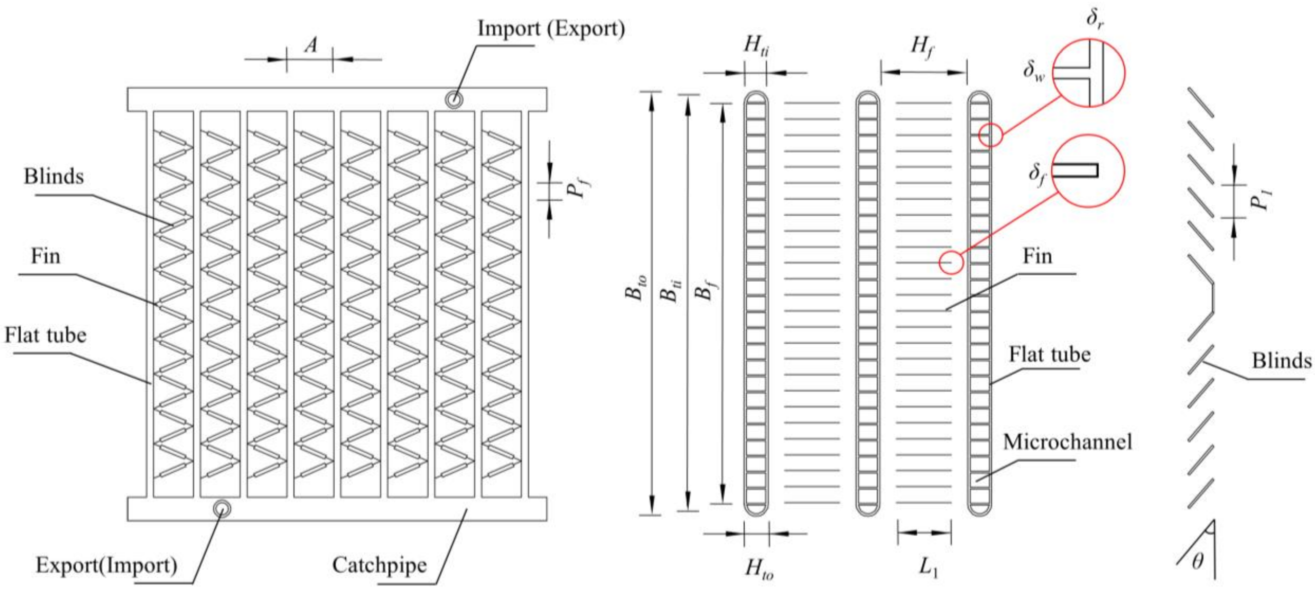

Figure 2. Structural dimensions of the microchannel heat exchanger.

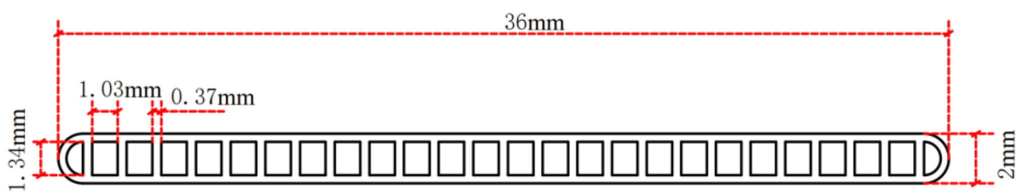

Figure 3. Single flat pipe size.

3.1.1. Parameters of the Air Side outside the Flat Pipe

For a single planar tube of unit length ΔL, the windward surface area is:

$$A_f = (H_f + H_{to}) \cdot \Delta L \tag{1}$$

The effective area to the wind is:

$$A_{fe} = A_f - H_{to} \cdot \Delta L - \frac{\Delta L}{P_f}\left[H_f \cdot \delta_f + (P_f - \delta_f) \cdot \delta_f\right] \tag{2}$$

The air velocity between the fins, v_a, can be calculated based on the given face velocity of the air, v, and the heat exchanger design parameters.

$$v_a = \frac{v(H_f + H_{to}) \times 2P_f}{H_f \times 2P_f - 2\sqrt{H_f^2 + P_f^2}\delta_f} \tag{3}$$

The maximum flow rate of air between the ailerons $v_{a\max}$ is

$$v_{a\max} = v_a \frac{A_f}{A_{fe}} \tag{4}$$

The area of heat transfer from the outer surface of the planar tube in direct contact with air is:

$$A_{\mathrm{N}1} = \left[2(B_{to} - H_{to}) \cdot \left(1 - \frac{\delta_f}{P_f}\right) + \pi H_{to}\right] \cdot \Delta L \tag{5}$$

The heat transfer area of the louvered fins in contact with the air is

$$A_{\mathrm{N}2} = 2B_f \frac{\Delta L}{P_f}\left(H_f - 2\delta_f\right) \tag{6}$$

The total surface area for heat exchange is

$$A_{\mathrm{N}} = A_{\mathrm{N}1} + A_{\mathrm{N}2} \tag{7}$$

The area without the rib side is as follows:

$$A = [2(B_{to} - H_{to}) + \pi H_{to}]\Delta L \tag{8}$$

3.1.2. The Work-Side Parameters in the Flat Tube

The heat transfer area for the direct heat transfer of refrigerant through the flat tubes is defined as follows:

$$A_{t1} = 2(B_{ti} - H_{ti} - N_w \delta_w)\Delta L + \pi H_{ti} \Delta L \tag{9}$$

The refrigerant transfers heat to the sheet, which in turn transfers heat to the flat tube for heat exchange with the air in the heat transfer area.

$$A_{t2} = 2N_w H_{ti} \Delta L \tag{10}$$

The total area for heat exchange between the refrigerant and air:

$$A_t = A_{t1} + A_{t2} \tag{11}$$

3.2. Design of the Heat Pipe Evaporator

3.2.1. The Calculation of the Heat Transfer Coefficient on the Air Side

The air-side heat transfer coefficient, h_{ae}, is given by the correlation proposed by Kim and Bullard [29]:

$$h_{ae} = jRe_{Lp} {Pr_{ae}}^{1/3} \frac{\lambda_{ae}}{P_l} \tag{12}$$

where the louvered fin j-factor correlation equation is

$$j = Re_{Lp}{}^{-0.487}(\frac{\theta}{90})^{0.257}(\frac{P_f}{P_l})^{-0.13}(\frac{H_f}{P_l})^{-0.29}(\frac{B_f}{P_l})^{-0.235}(\frac{L_1}{P_l})^{0.68}(\frac{\delta_w}{P_l})^{-0.279}(\frac{\delta_f}{P_l})^{-0.05} \tag{13}$$

The Fanning friction factor is given by:

$$f = Re_{LP}{}^{-0.781}(\frac{\theta}{90})^{0.444}(\frac{P_f}{P_l})^{-1.682}(\frac{H_f}{P_l})^{-1.22}(\frac{B_f}{P_l})^{0.818}(\frac{L_1}{P_l})^{1.97} \tag{14}$$

where Re_{Lp} is the air-side Reynolds number based on the louver pitch and is calculated as:

$$Re_{Lp} = \frac{\rho_a v_{a\max} P_l}{\mu_a} \tag{15}$$

The air-side fin efficiency is obtained from:

$$\eta_f = \frac{th(ml)}{ml} = \frac{th\left[\sqrt{\frac{2h_{ae}(B_f+\delta_f)}{\lambda_t \delta_w B_f}} \cdot \frac{H_f}{2}\right]}{\sqrt{\frac{2h_{ae}(B_f+\delta_f)}{\lambda_t \delta_w B_f}} \cdot \frac{H_f}{2}} \tag{16}$$

The total efficiency of the air-side rib wall:

$$\eta_o = \frac{A_{\mathrm{N1}} + \eta_f A_{\mathrm{N2}}}{A_{\mathrm{N}}} \tag{17}$$

Ribbing factor:

$$\beta_1 = \frac{A_{\mathrm{N}}}{A} \tag{18}$$

3.2.2. The Coefficient of Heat Transfer on the Working-Mass Side

The heat exchange of the circulating mass in the heat pipe evaporator can be split into three states. First, the working mass enters the evaporator of the heat pipe from the descending liquid tube and enters a subcooled liquid state, at which point the apparent heat exchange between the working mass of the liquid and the air will take place. Once the heat has been absorbed, the work material reaches boiling point and enters the two-phase zone to begin the heat transfer by phase change. In the phase change heat transfer process, the dryness of the working mass gradually increases and eventually evaporates completely into a gas and becomes superheated, thereby achieving the sensible heat exchange of the working mass of the gas.

(a) Subcooled liquid zone

The total mass flow rate of the working mass is G = 0.606 kg/s. The number of single-row flat tubes is 230, and the mass flow rate per unit area of the working mass equivalent in a single tube G_{vl} is 78.5 kg/m^2·s.

The Reynolds number of the refrigerant in the subcooled liquid zone, Re_{vl}, is calculated as

$$Re_{vl} = \frac{G_{vl} D_t}{\mu_{vl}} \tag{19}$$

where D_t is the hydraulic diameter of the flat tube.

The heat transfer coefficient h_{vl} of the refrigerant in the supercooled liquid zone is given by Bhatti and Shah [30]. The proposed correlation is given by

$$Re_c = \frac{4650}{V_r} \tag{20}$$

Among them

$$V_r = \frac{m+1}{m}\frac{n+1}{n} \tag{21}$$

$$m = 1.7 + 0.5\alpha^{-1.4} \tag{22}$$

where α is the aspect ratio of the microchannel when $\alpha < 1/3$, $n = 2$; when $\alpha \geq 1/3$, $n = 2 + 0.3 \times (\alpha - 1/3)$.

It has been calculated that Re_{v1} (523.3) < Re_c (2251.2) and the flow state of the working mass in the tube is in the laminar flow region, while the corresponding Nu calculation formula is as follows.

$$Nu = 8.325(1 - 2.2041\alpha + 3.0853\alpha^2 - 2.4756\alpha^3 + 1.0578\alpha^4 - 0.186\alpha^5) \tag{23}$$

The heat transfer coefficient h the refrigerant side of the subcooled liquid mass in the heat pipe evaporator h_{vl} is expressed as

$$h_{vl} = \frac{Nu_{vl} \times \lambda_{vl}}{D_t} \tag{24}$$

(b) Two-phase zone

The heat transfer coefficient h_{vr} the refrigerant in the two-phase region is given by the correlation propsed by Kandlikar [31]. The proposed correlation is expressed as follows:

$$h_{vr,nbd} = 0.6683Co^{-0.2}(1-x)^{0.8}f_2(Fr_{lo})h_{lo} + 1058Bo^{0.7}(1-x)^{0.8}F_{fl}h_{lo} \tag{25}$$

$$h_{vr,cbd} = 1.1360Co^{-0.9}(1-x)^{0.8}f_2(Fr_{lo})h_{lo} + 667.2Bo^{0.7}(1-x)^{0.8}F_{fl}h_{lo} \tag{26}$$

$$h_{vr} = (h_{vr,nbd}, h_{vr,cbd})_{\max} \tag{27}$$

where Co—convection number;

x—dryness;

Fr_{lo}—liquid phase Fr number;

Bo—boiling number;

h_{lo}—liquid phase heat transfer coefficient, W/(m^2·K);

f—friction factor.

For R22, F_{fl} is taken as 2.2 and each other parameter is defined as

$$Co = (\frac{\rho_{vg}}{\rho_{vl}})^{0.5}(\frac{1-x}{x})^{0.8} \tag{28}$$

$$Fr_{lo} = \frac{G_{vr}{}^2}{\rho_{vl}{}^2 g D_t} \tag{29}$$

$$f_2(Fr_{lo}) = (25Fr_{lo}, 1.0)_{\min} \tag{30}$$

$$Bo = \frac{q''}{G_{vr} r_{vl}} \tag{31}$$

$$h_{lo} = 3.66\lambda_{vl}/D_t \qquad Re_{vr} \leq 1600 \tag{32}$$

$$h_{lo} = \frac{(Re_{vr} - 1000)Pr_{vl}(f/2)(\lambda_{vl}/D_t)}{1 + 12.7(Pr_{vl}{}^{2/3} - 1)(f/2)^{0.5}} \qquad 1600 \leq Re_{vr} \leq 10^4 \tag{33}$$

$$h_{lo} = \frac{Re_{vr}Pr_{vl}(f/2)(\lambda_{vl}/D)}{1 + 12.7(\mathrm{Pr}_{vl}^{2/3} - 1)(f/2)^{0.5}} \qquad 10^4 \leq Re_{vr} \leq 5 \times 10^6 \tag{34}$$

$$f = [1.58In(Re_{vr}) - 3.28]^{-2} \tag{35}$$

(c) Superheated steam zone

The Reynolds number of the refrigerant in the superheated vapor zone, Re_{vg}, is calculated as

$$Re_{vg} = \frac{G_{vg}D_t}{\mu_{vg}} \tag{36}$$

where G_{vg} is the gas-phase's working mass flow rate, kg/s.

The heat transfer coefficient in the superheated steam zone is calculated using Gnielinsky's [32] predicted correlation equation; when Re_{vg} (245.5) ≤ 2300, Nu takes the value of

$$Nu = 4.36 \tag{37}$$

The heat transfer coefficient h_{vg} on the refrigerant side of the superheated vapor state in the heat pipe evaporator is expressed as

$$h_{vg} = \frac{Nu_{vg} \times \lambda_{vg}}{D_t} \tag{38}$$

The calculated heat transfer coefficients for the three phase zones are weighted and averaged according to the proportion of each phase of the refrigerant in the heat exchanger, resulting in a refrigerant-side heat transfer coefficient h_{re}:

$$h_{re} = 0.1 \times h_{vl} + 0.85 \times h_{vr} + 0.05 \times h_{vg} \tag{39}$$

Rib efficiency of the flat tube:

$$\eta_r = \frac{th(ml)}{ml} = \frac{th\left[\sqrt{\frac{2h_{re}(\Delta L + \delta_w)}{\lambda_t \delta_w \Delta L}} \cdot \frac{H_{ti}}{2}\right]}{\sqrt{\frac{2h_{re}(\Delta L + \delta_w)}{\lambda_t \delta_w \Delta L}} \cdot \frac{H_{ti}}{2}} \tag{40}$$

Total rib wall efficiency:

$$\eta_{ro} = \frac{A_{t1} + \eta_r A_{t2}}{A_t} \tag{41}$$

Ribbing factor:

$$\beta_2 = \frac{A_t}{A} \tag{42}$$

Total heat transfer coefficient of heat pipe evaporator:

$$h_e = \frac{1}{\frac{1}{h_{ae}\beta_1\eta_o} + \frac{1}{h_{re}\beta_2\eta_{ro}}} \tag{43}$$

The calculation of the heat transfer area of the heat pipe evaporator is

$$A_e = \frac{Q_e}{h_e \Delta t_e} \tag{44}$$

where Δt_e is the heat transfer temperature difference given by:

$$\Delta t_e = \frac{t_2^e - t_1^e}{In\left(\frac{t_e - t_1^e}{t_e - t_2^e}\right)} \tag{45}$$

The final results for the evaporator are shown in Table 5.

Table 5. Evaporator design results.

Evaporator Heat Load Q_e (kW)	Air-Side Heat Transfer Coefficient h_{ae} (W/(m^2·K))	Refrigerant Heat Transfer Coefficient h_{re} (W/(m^2·K))	Total Heat Transfer Coefficient h_e (W/(m^2·K))	Heat Exchange Area A_e (m^2)	Single Tube Length L_e (mm)	Number of Flat Tubes
120.31	131.54	2033.18	658.53	25.58	1.6	230

3.3. Heat Pipe Condenser Design

The design calculations for the heat pipe condenser-side heat exchanger are similar to those for the evaporative side. Similarly, the air-side and refrigerant-side heat transfer coefficients are calculated, and the refrigerant-side heat transfer coefficients are also calculated according to the phase state using the corresponding correlation Equations (12)–(45). The final results for the condenser are shown in Table 6.

Table 6. The results for the condenser design.

Condenser Heat Load Q_c (kW)	Air-Side Heat Transfer Coefficient h_{ac} (W/(m^2·K))	Refrigerant Heat Transfer Coefficient h_{rc} (W/(m^2·K))	Total Heat Transfer Coefficient h_c (W/(m^2·K))	Heat Exchange Area A_c (m^2)	Single Tube Length L_c (mm)	Number of Flat Tubes
120.31	169.07	1748.2	461.60	32.58	2.1	230

3.4. Calculation of Pressure Drop in Heat Pipe System

The working medium in the micro-channel heat pipe system flow's pressure drop mainly contains the following four forms: (1) a gravitational pressure drop due to the change in the position of the working medium and the change in potential energy; (2) an accelerated pressure drop due to the conversion between kinetic energy and the pressure energy of the working medium; (3) a frictional pressure drop caused by friction between the working medium in the flow process and the pipe wall; (4) a pressure drop due to sudden expansion and contraction of the heat exchanger collector tube at the connection with the gas and liquid tubes.

3.4.1. Frictional Pressure Drop

The frictional pressure drop in the single-phase zone is calculated according to the formula of Gnielinski V [32]. The empirical equation is calculated as

$$\Delta P_{f(l/g)} = f\frac{l}{D_t}\frac{{G_{v(l/g)}}^2}{2\rho_{v(l/g)}} \tag{46}$$

$$f = \frac{64}{\mathrm{Re}_{v(l/g)}}\mathrm{Re}_{v(l/g)} \leq 2300 \tag{47}$$

$$f = 0.3164 \times \mathrm{Re}_{v(l/g)}{}^{-0.25}\mathrm{Re}_{v(l/g)} > 2300 \tag{48}$$

The frictional pressure drop in the two-phase zone is calculated with reference to Friedel L [33]. The empirical equation is calculated as

$$\Delta P_{fr} = \frac{{G_{vr}}^2 fl}{2\rho_i D_t}(E + \frac{3.24FH}{Fr^{0.045}We^{0.035}}) \tag{49}$$

$$E = (1-x)^2 + x^2\frac{\rho_{vl}{\mathrm{Re}_{vg}}^{-0.25}}{\rho_{vg}{\mathrm{Re}_{vl}}^{-0.25}} \tag{50}$$

$$F = x^{0.78}(1-x)^{0.224} \tag{51}$$

$$H = (\frac{\rho_{vl}}{\rho_{vg}})^{0.91}(\frac{\mu_{vg}}{\mu_{vl}})^{0.19}(1-\frac{\mu_{vg}}{\mu_{vl}})^{0.7} \tag{52}$$

$$\rho_i = (\frac{x}{\rho_{vg}} + \frac{1-x}{\rho_{vl}})^{-1} \tag{53}$$

$$Fr = \frac{G_{vr}^2}{gD_t\rho_i^2} \tag{54}$$

$$We = \frac{G_{vr}^2 D_t}{\sigma\rho_i} \tag{55}$$

where l—pipe length, m;
Fr—Froude number;
We—Weber numbers;
ρ_i—combined density of the two refrigerants, kg/m^3;
σ—surface tension, N/m.

3.4.2. Gravitational Pressure Drop

$$\Delta P_g = \rho_i g H \tag{56}$$

where H is the height of the working mass flowing through, m.

3.4.3. Accelerated Pressure Drop

The model proposed by Carey [34] was chosen for the calculation, which is given as follows:

$$\Delta P_a = G^2 \left\{ \left[\frac{x^2}{a\rho_{vg}} - \frac{(1-x)^2}{(1-a)\rho_{vl}} \right]_{in} - \left[\frac{x^2}{a\rho_{vg}} - \frac{(1-x)^2}{(1-a)\rho_{vl}} \right]_{out} \right\} \tag{57}$$

where a is the vacuolation factor, calculated from Equation (58).

$$a = \frac{1}{1 + 0.28[(1-x)x]^{0.64} (\frac{\rho_{vg}}{\rho_{vl}})^{0.86} (\frac{\mu_{vg}}{\mu_{vl}})^{0.07}} \tag{58}$$

3.4.4. Pressure Drop Caused by Sudden Expansion and Contraction

The sudden expansion-based pressure drop, ΔP_e, is given by the correlation proposed by Gnielinski V [32]:

$$\Delta P_e = K_e \frac{\rho_i V^2}{2} = \left[(1-\sigma)^2 - 0.4\sigma \right] \frac{\rho_i V^2}{2} \tag{59}$$

The sudden contraction-based pressure drop, ΔP_c, is given by the correlation proposed by Friedel L [33]:

$$\Delta P_c = K_c \frac{\rho_i V^2}{2} = (0.8 - 0.4\sigma^2) \frac{\rho_i V^2}{2} \tag{60}$$

where K_e—coefficient of sudden expansion loss;
K_c—coefficient of sudden shrinkage loss;
V—velocity of working mass flow, m/s;
σ—area ratio.

The phase states of the refrigerant present in the heat pipe heat exchanger are the subcooled liquid state, the gas–liquid two-phase zone, and the superheated gas state. For the single-phase zone, there is no accelerated pressure drop and its length is very short, so the pressure drop due to gravity is ignored. For the pressure drop of the refrigerant in the gas and liquid tubes, there is also no accelerated pressure drop, and the respective frictional pressure drops are calculated based on the physical parameters of the working masses in the gas and liquid tubes, respectively. Due to the horizontal arrangement of the gas and liquid tubes, there is no pressure drop caused by gravity. The calculation results are shown in Table 7.

Table 7. Pressure drop of refrigerant flow in heat pipe system.

	Heat Pipe Evaporator	Heat Pipe Condenser	Air Ducts	Liquid Tube
Frictional pressure drop (Pa)	9157.4	12,630.2	8.2	699.3
Accelerated pressure drop (Pa)	−1615.9	1636.1		
Gravitational pressure drop (Pa)	1561	−1597.2		
Sudden expansion (Pa)	628.7	6855.6		
Sudden contraction (Pa)	−28	−2.6		
Gas–liquid separator and reservoir (bar)		0.5		
Total system refrigerant resistance (bar)		0.799		

4. Performance Evaluation Methods

The performance of the evaporative condensing- and microchannel-split heat pipe units can be evaluated according to the temperature drop, cooling output, and COP. The temperature drop is the temperature difference between the primary air return temperature and the supply air temperature.

$$t_{drop} = t_{1,p} - t_{2,p} \tag{61}$$

In the equation: $t_{1,p}$—the primary air inlet's dry-bulb temperature, °C;
$t_{2,p}$—the primary air outlet's dry-bulb temperature, °C.

According to the formula provided by the ASHRAE Standard [35], the cooling output can be expressed as:

$$Q_{cooling} = c_{p,a}\rho_a M_1(t_{1,p} - t_{2,p}) \tag{62}$$

In the equation, $c_{p,a}$—Air constant pressure specific heat capacity, kJ/(kg·K);
ρ_a—Outlet air density, kg/m^3;
M_1—Primary air volume, m^3/h.

The COP [35] is expressed as the ratio of the cooling output ($Q_{cooling}$) to the total power consumption (W) of the air cooler, given by:

$$\text{COP} = \frac{Q_{cooling}}{W_{fan} + W_{pump,w} + W_{pump,f} + W_m} \tag{63}$$

In the equation, W_{fan}—Fan power, kW;
$W_{pump,w}$—Power of water pump, kW;
$W_{pump,f}$—Power of fluorine pump, kW;
W_m—Power of mechanical cooling, kW.

5. Testing Processes, Results, and Discussion

5.1. Optimal Liquid-Filling Rate for Power Heat Pipe Systems

The heat pipe's filling rate R is defined as the ratio of the volume of the liquid-phase working mass filled to the volume inside the evaporator tube [36].

$$R = V_1/V_e \tag{64}$$

In the equation: V_1—the volume of the liquid phase workpiece charged, mm^3;
V_e—the volume inside the evaporator tube, mm^3.

For the optimum liquid-filling rate experiment, the unit was operated in power heat pipe mode with the primary fan, secondary fan, and fluorine pump switched on. The laboratory-simulated working conditions are shown in Table 8. The mass of the liquid-phase workpiece in the heat pipe was first charged with 10 kg and changed with an adjustment rate of 2 kg each time. In each test, the inlet and outlet air temperature of the unit and the energy consumption of each component were recorded, and the cooling capacity and COP of the system were calculated for different charging rates. The effects of the different charging rates on the performance of the heat pipe system are shown in Figure 4.

Table 8. Experimental working parameters of optimal liquid-filling rate.

Indoor Environmental Parameters		Outdoor Environmental Parameters		Secondary Air Volume (m^3/h)	Primary Air Volume (m^3/h)	Filled with Liquid-Phase Quality of Workpiece (kg)	Liquid-Filling Rate (%)
Inlet Air Dry Bulb Temperature (°C)	Inlet Air Wet Bulb Temperature (°C)	Inlet Air Dry Bulb Temperature (°C)	Inlet Air Wet Bulb Temperature (°C)				
38.0	22.0	14.0	10.6	66,000	30,000	10	71.5
						12	85.8
						14	100.0
						15	107.2
						16	114.4
						17	121.6
						18	128.7

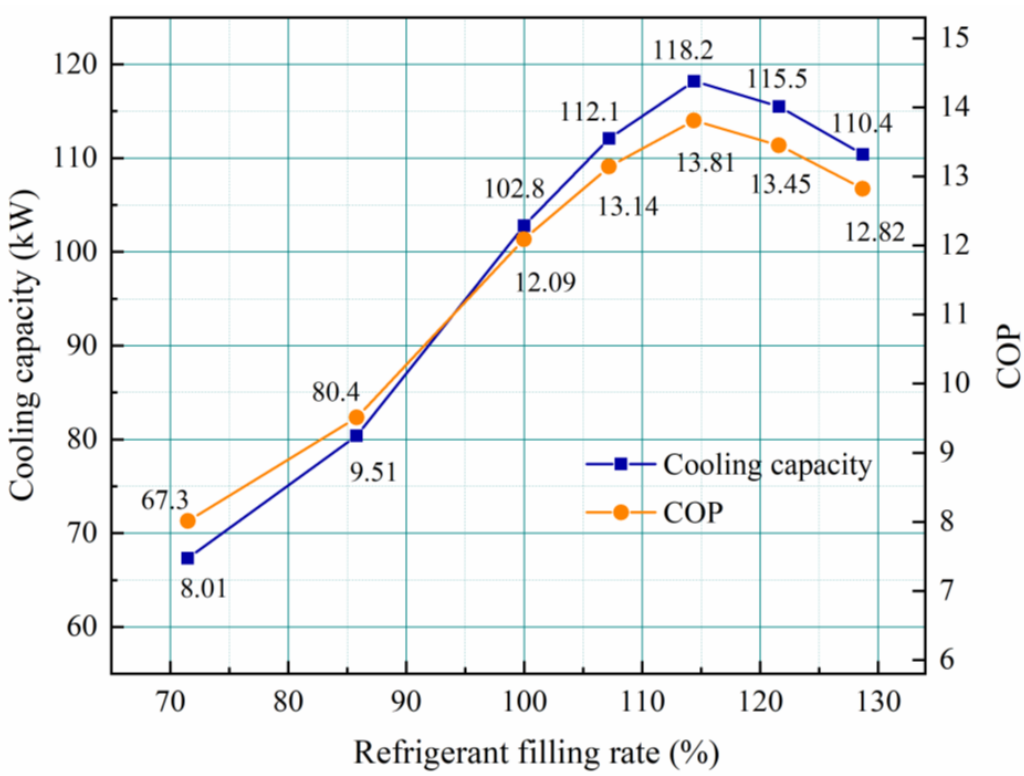

Figure 4. Effect of different liquid-filling rates on the performance of heat pipe system.

As shown in Figure 4, with the increase in the liquid charge rate of the heat pipe system, the cooling capacity of the unit tends to increase first and then decrease. When the liquid charge rate is 114.4%, the cooling capacity of the unit reaches the experimental maximum of 118.2 kW, and the COP of the system is 13.81. Since the phase heat transfer of the refrigerant is much higher than the sensible heat transfer, regardless of whether the liquid charge rate is too high or too low, the sensible heat transfer of the single-phase mass in the heat pipe will occupy more heat transfer space, thus affecting the heat transfer of the heat pipe system. It has been found that the system can be maintained at optimal operating conditions when the liquid-filling rate is 114.4%.

5.2. Energy-Saving Analyses of the Hybrid Cooling Systems

The annual dry-bulb temperature distribution in Xi'an is shown in Figure 5. There are about 4137 h of outdoor air dry-bulb temperatures lower than 14 °C throughout the year, accounting for 47.2%. There are about 538 h of outdoor dry-bulb temperatures higher than 14 °C and wet-bulb temperatures lower than 13°C throughout the year, accounting for 6.1%. The unit can be turned operated in three operating modes throughout the year to reduce the system's energy consumption. The monthly running time statistics of the unit under the three operating modes are shown in Figure 6.

As shown in Figure 6, under Xi'an operating conditions, the unit mainly operates in mechanical cooling mode from June to September when both dry- and wet-bulb outdoor air temperatures are high. From November to March, when the dry-bulb temperature of the outdoor air is low, the unit mainly operates in the power heat pipe mode. In addition, in the transitional season of April and October, the operating hours for using a natural cooling source can be further enhanced with the pre-cooling of the wet film.

Table 9 shows the total energy consumption of the hybrid cooling system. The COP of the system in power heat pipe mode can reach more than 14, and the annual average COP of the system is 9.43. The total energy consumption of the hybrid system is compared with the energy consumption of a conventional server room air conditioning system in Table 10. The results show that the hybrid cooling system described in this paper is more efficient than the conventional server room's air conditioning system, with energy savings of about 62%. Therefore, the hybrid cooling system can significantly reduce the cooling-based energy consumption of data centers.

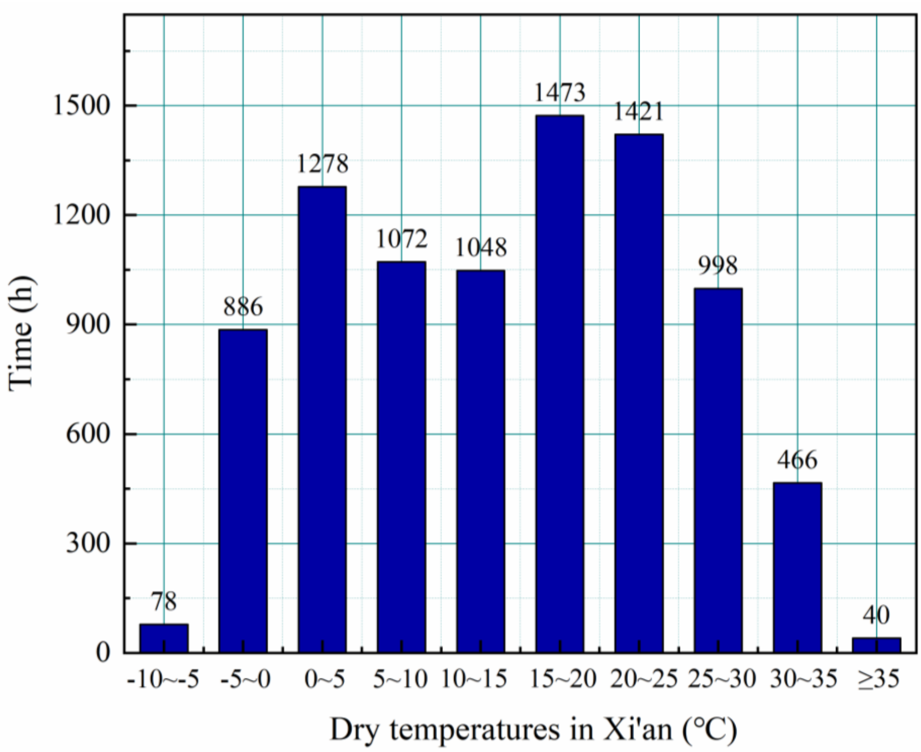

Figure 5. Number of hours per year with these dry-bulb temperatures in Xi'an.

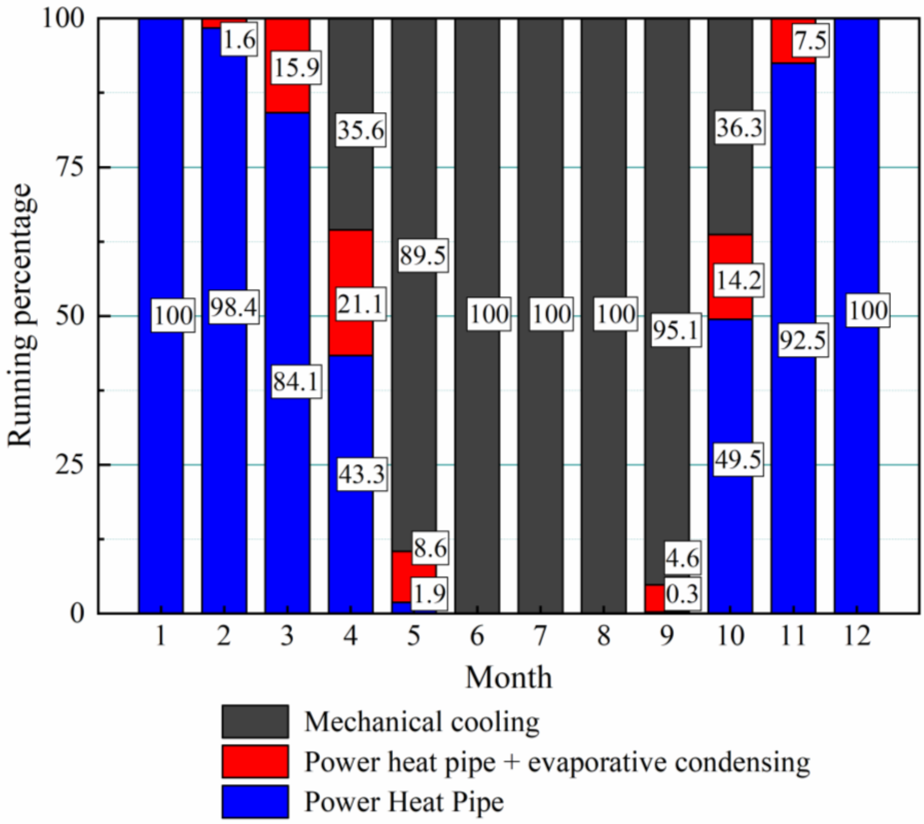

Figure 6. Monthly running time ratio of the three operation modes.

Table 9. Annual energy consumption for system.

Temperature (°C)	≤11	11~14	14~18	18~22	22~26	26~30	≥30
Working time (h)	3523.6	628.8	1093.4	1157.6	1052.2	798.4	506
Cooling capacity of heat pipe (kW)	120	120	94.49	32.96	3.28	0	0
Cooling capacity of mechanical cooling (kW)	0	0	25.51	87.04	116.72	120	120
Total cooling capacity (kW)	120	120	120	120	120	120	120
Total heat pipe power consumption (kW)	7.63	7.83	6.47	2.15	1.98	0	0
Total power consumption of evaporative condensation (kW)	0.47	0.68	0.75	0.75	0.75	0.75	0.75
Total power consumption of mechanical cooling (kW)	0	0	9.66	23.74	29.35	32.68	34.34
Total power consumption (kW)	8.10	8.51	16.88	26.64	32.08	33.43	35.09
COP	14.81	14.10	7.11	4.50	3.74	3.59	3.42
Average COP				9.43			

Table 10. Comparison of annual energy consumption.

Cooling System	Rated Cooling Capacity (kW)	Annual Energy Consumption (kWh)	Annual Average COP	Energy Saving Proportion
CRAC	120	328,545	3.4	3.4
hybrid cooling system	120	124,726	9.43	62.04%

6. Conclusions

This paper presents a hybrid cooling system that effectively uses natural cooling sources to reduce data centers' cooling-based energy consumption, wherein the system combines evaporative condensing technology and a microchannel-split heat pipe. The microchannel-split heat pipe system was designed in detail and the energy-saving effect of the system was tested and analyzed according to the weather conditions of Xi'an. The conclusions obtained are as follows.

(1) This paper describes a refrigeration system with evaporative condensing & microchannel separated heat pipe coupling and switching points of outdoor state parameters for the three operation modes of the system are given. Under operating conditions corresponding to Xi'an, the annual operation percentages of the power heat pipe mode, The power heat pipe mode, evaporative condensing + power heat pipe mode and mechanical refrigeration make-up cooling mode accounted for 47.2%, 6.1% and 46.7% of the annual operation, respectively.

(2) Based on the Xi'an data center's design parameters, the microchannel-separated heat pipe system was designed in detail. The optimal liquid-filling rate of the heat pipe system was determined to be 114.4% through experimental testing.

(3) The energy consumption rate of a hybrid cooling system in a typical year in Xi'an was given and compared with that of a conventional vapor compression system. The results show that the annual energy consumption of the hybrid cooling system is 124,726 kWh with an average COP of 9.43. The annual electricity consumption of the hybrid cooling system is 62.04% less than that of the conventional vapor compression system. The cooling system incorporating evaporative condensing and microchannel-separated heat pipe coupling has great potential to reduce energy consumption in data centers.

Author Contributions: Writing—original draft, Y.W.; Methodology, X.H.; Software, C.D. and G.M.; Resources, X.H. and X.T.; Data curation, Y.D.; Writing—review & editing, J.C. All authors have read and agreed to the published version of the manuscript.

Funding: This research was funded by (1) Shenzhen Science and Technology Program (KCXFZ2020 1221173409026) and (2) the National Key Research and Development Program (2016YFC0700404).

Conflicts of Interest: No conflict of interest exits in the submission of this manuscript, and manuscript is approved by all authors for publication.

References

1. *China Green Data Center Development Report (2020)*; Electronics Association: Beijing, China, 2021.
2. Department of Information and Communication Development, Ministry of Industry and Information Technology. *National Data Center Application Development Guidelines (2018)*; Department of Information and Communication Development, Ministry of Industry and Information Technology: Beijing, China, 2018.
3. Ebrahimi, K.; Jones, G.F.; Fleischer, A.S. A review of data center cooling technology, operating conditions and the corresponding low-grade waste heat recovery opportunities. *Renew. Sustain. Energy Rev.* **2014**, *31*, 622–638. [CrossRef]
4. Meijer, G.I. Cooling energy-hungry data centers. *Science* **2010**, *328*, 318–319. [CrossRef] [PubMed]
5. Hu, J.X.; Zhou, Q.L.; Gu, G.D. Exploration and research on energy consumption status and energy saving direction of data center. *Comput. Program. Skills Mainten.* **2019**, *4*, 93–95. (In Chinese)
6. Siriwardana, J.; Jayasekara, S.; Halgamuge, S.K. Potential of air-side economizers for data center cooling: A case study for key Australian cities. *Appl. Energy* **2013**, *104*, 207–219. [CrossRef]
7. Yuan, X.; Zhou, X.; Pan, Y.; Kosonen, R.; Cai, H.; Gao, Y.; Wang, Y. Phase change cooling in data centers: A review. *Energy Build.* **2021**, *236*, 110764. [CrossRef]
8. Zhang, K.; Zhang, Y.; Liu, J.; Niu, X. Recent advancements on thermal management and evaluation for data centers. *Appl. Therm. Eng.* **2018**, *142*, 215–231. [CrossRef]
9. Miller, R.; Google's Chiller-less data center. Data Center Knowledge. Available online: https://www.datacenterknowledge.com/archives/2009/07/15/googles-chiller-less-data-center/ (accessed on 15 July 2009).
10. Park, J.; Open Compute Project Data Center v1.0. The Open Compute Project. 2011. Available online: https://docshare.tips/open-compute-project-data-center-v10 (accessed on 22 October 2022).
11. Mu, Z.H.; Wang, Y. Air conditioning design of cloud computing data center in Zhongwei, Ningxia. *HVAC* **2016**, *46*, 23–26.
12. Ham, S.W.; Kim, M.H.; Choi, B.N.; Jeong, J.W. Energy saving potential of various air-side economizers in a modular data center. *Appl. Energy* **2015**, *138*, 258–275. [CrossRef]
13. Pan, J.; Wang, K.Y.; Wang, C.P. Development trend of cooling technology in data centers. *Telecommun. Inf.* **2019**, *2*, 43–44. (In Chinese)
14. Niu, X.; Xia, C.; Sun, G. Air conditioning system design with lake water cooling technology of a data center in Qiandao Lake. *Heat. Ventilat. Air Condit.* **2016**, *46*, 14–17.
15. Lee, K.P.; Chen, H.L. Analysis of energy saving potential of air-side free cooling for data centers in worldwide climate zones. *Energy Build.* **2013**, *64*, 103–112. [CrossRef]
16. Liu, C. How is PUE less than 1.10 achieved? Uncovering the Tencent T-block Data Center. *Ups Appl.* **2016**, *6*, 16–18.
17. Weerts, B.A.; Gallaher, D.; Weaver, R.; Vangeet, O. Green data center cooling: Achieving 90% reduction: Airside economization and unique indirect evaporative cooling. In Proceedings of the 2012 IEEE Green Technologies Conference, Tulsa, OK, USA, 19–20 April 2012; pp. 1–6.
18. DOE. NSIDC Data Center: Energy Reduction Strategies Airside Economization and Unique Indirect Evaporative Cooling. U.S. Department of Energy. Federal Energy Management Program. 2012. Available online: https://www.energy.gov/eere/femp/downloads/nsidc-data-center-energy-reduction-strategies (accessed on 22 October 2022).
19. Bi, Y.; Wang, Y.; Ma, X.; Zhao, X. Investigation on the energy saving potential of using a novel dew point cooling system in data centres. *Energies* **2017**, *10*, 1732. [CrossRef]
20. Tozer, R.; Flucker, S. zero refrigeration for data centres in the USA. *ASHRAE Trans.* **2012**, *118*, 261–268.
21. Ndukaife, T.A.; Nnanna, A.G.A. Optimization of Water Consumption in Hybrid Evaporative Cooling Air Conditioning Systems for Data Center Cooling Applications. *Heat Transf. Eng.* **2019**, *40*, 559–573. [CrossRef]
22. Ling, L.; Zhang, Q.; Yu, Y.; Liao, S. A state-of-the-art review on the application of heat pipe system in data centers. *Appl. Therm. Eng.* **2021**, *199*, 117618. [CrossRef]
23. Ding, T.; Chen, X.; Cao, H.; He, Z.; Wang, J.; Li, Z. Principles of loop thermosyphon and its Application in data center cooling systems: A review. *Renew. Sustain. Energy Rev.* **2021**, *150*, 111389. [CrossRef]
24. Li, Q.H.; Huang, H.; Zhang, Z.B. Performance experiment of heat pipe type air. *Heat. Vent. Air Cond.* **2010**, *40*, 145–148. (In Chinese)
25. Han, X.L.; Tu, S.P.; Li, X.Z. Calculation of natural cooling unit for fluorine pumps used in data center. *Refrigeration* **2018**, *37*, 75–79. (In Chinese)

26. Lin, Y.C.; Liu, J.P.; Xu, X.W.; Liu, Z.; Li, G.L. Experimental research on air conditioning system of a computer room based on refrigerant pump pressurization. *Refrigeration* **2020**, *41*, 83–88. (In Chinese)
27. Xu, Z.; Zhang, Y.; Li, B.; Wang, C.C.; Li, Y. The influences of the inclination angle and evaporator wettability on the heat performance of a thermosyphon by simulation and experiment. *Int. J. Heat Mass Transf.* **2018**, *116*, 675–684. [CrossRef]
28. *GB 50174-2017*; Data Center Design Specification. China Planning Press: Beijing, China, 2017.
29. Kim, M.H.; Bullard, C.W. Air-side thermal hydraulic performance of multi-louvered fin aluminum heat exchangers. *Int. J. Refrig.* **2002**, *25*, 390–400. [CrossRef]
30. Bhatti, M.S.; Shah, R.K. Turbulent and transition flow convective heat transfer in ducts. In *Handbook of Single-Phase Convective Heat Transfer*; Kakaç, S., Shah, R.K., Aung, W., Eds.; Wiley: New York, NY, USA, 1987; pp. 4.1–4.166.
31. Kandlikar, S.G.; Steinke, M.E. Predicting heat transfer during flow boiling in minichannels and microchannels. *ASHRAE Trans.* **2003**, *109*, 667.
32. Gnielinski, V. New Equations for Heat and Mass Transfer in Turbulent Pipe and Channel Flows. *Int. Chem. Eng.* **1976**, *16*, 359–368.
33. Friedel, L. Improved Friction Pressure Drop Correlation for Horizontal and Vertical Two-Phase Pipe Flow. *Proc. Eur. Two-Phase Flow Group Meet. Ispra Italy* **1979**, *18*, 485–491.
34. Zhang, P.; Wang, B.; Shi, W.; Han, L.; Li, X. Modeling and performance analysis of a two-phase thermosyphon loop with partially/fully liquid-filled downcomer. *Int. J. Refrig.* **2015**, *58*, 172–185. [CrossRef]
35. ASHRAE. *ASHRAE Handbook Fundamentals Volume: SI Edition*; American Society of Heating, Refrigerating and Air-Conditioning Engineers: Atlanta, GA, USA, 2009; Chapter 4; p. 4.18.
36. Jin, A.C.; Shi, Z.C.; Shao, S.Q.; Tian, C.Q. Experimental study on the performance of split heat pipe air conditioner using microchannel heat exchanger. *Low Temp. Supercond.* **2016**, *44*, 64–68.